Study of the Far Wake of a Large Ship

M. GILMAN

Oceanographic Center, Nova Southeastern University, Dania Beach, Florida

A. SOLOVIEV

Oceanographic Center, Nova Southeastern University, Dania Beach, and Rosenstiel School of Marine and Atmospheric Science, University of Miami, Miami, Florida

H. GRABER

Rosenstiel School of Marine and Atmospheric Science, University of Miami, Miami, Florida

(Manuscript received 19 April 2010, in final form 9 September 2010)

ABSTRACT

A large dataset of high-resolution photographic images of far wakes of a volunteer observing ship (Royal Caribbean's *Explorer of the Seas*) has been acquired under various meteorological conditions and ship operation modes. This work presents the description of instrumentation, methodology, and the results of the experiment. Environmental and ship operation factors that affect appearance and geometric properties of ship wakes in photographic and satellite-based radar images have been analyzed. The photo imagery reveals an asymmetry of the wake depending on wind direction relative to the ship course. In addition, a good agreement between the averaged shape of the wakes measured from the photographic images and a few available satellite-based radar images of the wake of the same ship has been found.

1. Introduction

The motivation to study far wakes of ships originates from the problem of remote (air and satellite based) ship detection and monitoring. The length of the centerline part of the ship wake (also called turbulent wake) can sometimes reach tens of kilometers, thus presenting significant additional opportunities for ship detection. After far wakes of ships were discovered in radar images of the National Aeronautics and Space Administration (NASA) *Seasat* satellite launched in 1978 (Fu and Holt 1982), several methods of data analysis aimed at ship detection were developed (see, e.g., Eldhuset 1996; Greidanus and Kourti 2006). A variety of topics are associated with the problem of ship detection, including ship hydrodynamics, surface films theory, radar imaging, image processing, and pattern recognition (see, e.g., Hyman 2000; Reed and Milgram 2002; Crisp 2004; Soomere 2007; Soloviev et al. 2008, and references therein). The infrared and optical imaging of ship wakes has also been an important experimental tool in studying different features of ship wakes (see, e.g., Garrett and Smith 1984; Munk et al. 1987; Brown et al. 1989; Zheng et al. 2001).

Recent advances in satellite-based imaging technology have provided images with a spatial resolution of 1–3 m, where fine features of wakes are detectable and measurable (Soloviev et al. 2010). This resolution is sufficient for determining the wake geometry with reasonable accuracy, considering a typical wake width of 100–200 m. The quantitative characteristics of the wake shape may give us insight into the ship dynamics and thus provide valuable additional information about the observed ships (see also Zilman et al. 2004).

Previous studies of far ship wakes rarely took into account environmental conditions and ship metrics. However, these parameters are important for the wake visibility and characteristics (see, e.g., Benilov et al. 2001). A proper account of environmental conditions can improve our understanding of this phenomenon. For example, it is well known that the higher the wind speed and sea state, the larger the image clutter, which may obscure the ship

Corresponding author address: A. Soloviev, Oceanographic Center, Nova Southeastern University, 8000 North Ocean Drive, Dania Beach, FL 33004.
E-mail: soloviev@nova.edu

DOI: 10.1175/2010JTECHO791.1

FIG. 1. Two locations, A and B, for the camera on *Explorer of the Seas*.

wake (Vachon 2006). It is important then to find correlations between the centerline (turbulent) ship wake characteristics visualized on photographic imagery and the ship and environmental data. For this purpose, photo images of ship wakes from the Royal Caribbean *Explorer of the Seas* cruise ship have been acquired. The hydrometeorological and ship operation data have been provided by the onboard laboratories maintained by the University of Miami (UM) Rosenstiel School of Marine and Atmospheric Science (RSMAS; information online at http://www.rsmas.miami.edu/rccl). Our experiment has no known parallels, either in the methodology, which involves a ship-borne astern-looking photographic camera, or in the amount of images collected and analyzed.

This work presents the methodology of data collection, the strategies of the data analysis, and the results of the experiment. The next section provides information about the setup of the experiment. The details of our image-processing procedures are given in section 3. The analysis of the measurements is presented in section 4. The formulas used for the calculation of wake shape can be found in the appendix.

2. Instrumentation

An astern-looking digital camera with a telephoto lens was installed on the aft mast of the Royal Caribbean *Explorer of the Seas* (Figs. 1 and 2). The purpose of this camera was to obtain high-resolution images of the ship's wake (see, e.g., Fig. 3) during an approximately 1-yr period.

The *Explorer of the Seas* is a large cruise ship (311-m length, 11.7-m draft, 38.6-m master beam, and 42-MW total thrust power). During this experiment, the ship was sailing from Miami, Florida, and New Jersey to the Caribbean, Bermuda Islands, New England, and eastern Canada.

The typical length of an *Explorer of the Seas* cruise ranges from 5 to 9 days. The camera was programmed to take images every 20 min, which allowed an 8-GB memory card to store images for the full cruise. The camera also includes a WT-3A wireless transmitter, which enables direct, cable-free image transfer to a laboratory computer (installed in the onboard meteorological laboratory). For the first half of the year, the camera was installed in portrait orientation. However, it turned out that in many cases

FIG. 2. A Nikon D-200 10-MP camera with an AF Nikkor 180-mm f/2.8D IF-ED lens placed in an Ocean Images underwater housing unit installed on the aft mast of the *Explorer of the Seas* (Fig. 1, location B).

FIG. 3. Example of a high-resolution ship wake image taken from the *Explorer of the Seas*. The image was taken from location B on the ship (Fig. 1) at 1909 UTC 16 Jun 2007; 35.4713°N, 72.0791°W. Ship speed was 22.5 kt, and the course was at 341.5°. Wind speed measurements from the bow anemometer provided by RSMAS are as follows: true wind speed of 13 kt and true wind direction of 291.6°.

the wake did not fit into the narrow field of view of the lens. This paper uses the results from the second half of the year where the camera orientation was changed to landscape.

RSMAS maintains oceanographic and meteorological laboratories on the *Explorer of the Seas*. In addition to the photo images of the ship wake, the information collected from *Explorer of the Seas* is as follows:

- ship speed, direction, heading, and geographical coordinates;
- hydrometeorological conditions: wind speed and direction, surface wave directional spectrum [from the Wave and Surface Monitoring System (WaMoS) radar], current velocity, water temperature and salinity, air temperature and humidity, radiometric sea surface temperature (SST), atmospheric pressure, and short- and longwave radiation; and
- fluorescence (a proxy for chlorophyll concentration).

The above data are recorded at 10-s intervals.

3. Data processing

At the first processing stage, the images taken during nighttime, heavy rain, or other unusable images (e.g., taken in ports) were sorted out manually. The subsequent processing targeted the following two features of the wake visible in the photographic images: wake asymmetry and wake shape.

a. Assigning wake asymmetry characteristics

The wake asymmetry data were obtained by reviewing photographic images of the wakes in the period from 9 June 2007 to 16 November 2007. The dataset was split into the following categories:

- "S wakes": only the starboard-side (right, if looking ahead, or left, if looking astern) wake boundary is

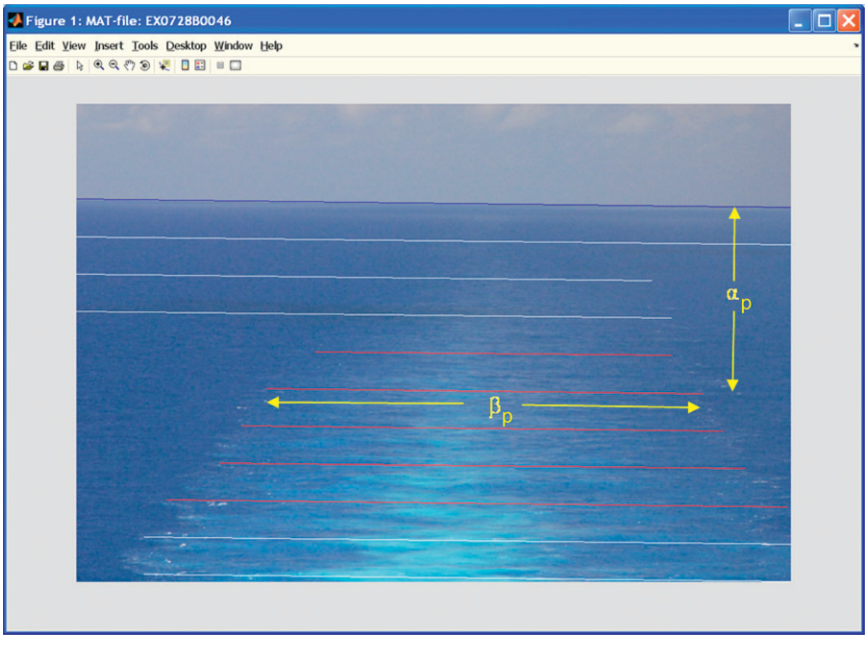

FIG. 4. Completed wake measurement: horizon-setting line is drawn (dark blue), wake measurement intervals are shown (red). The explanations for α_p and β_p can be found in the text. The white wake measurement intervals will be ignored because at least one of the wake boundaries is either not clearly seen (three top lines) or beyond the image (bottom two lines).

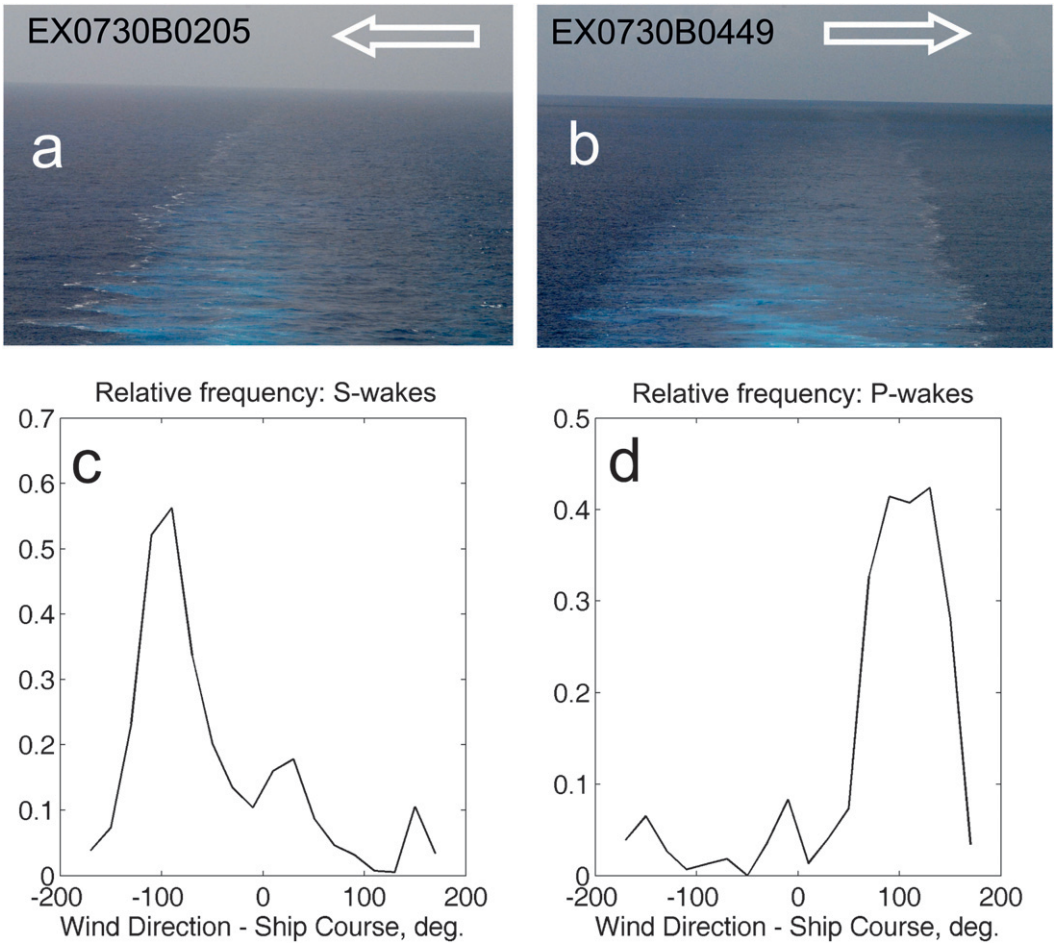

FIG. 5. Wake asymmetry vs relative wind direction. (top) Examples of asymmetric wakes (the arrow shows the wind direction relative to the wake). (a) S wake: 1630:03 UTC 23 Jul 2007, ship course of 176.1°, ship speed of 22.2 kt, wind direction of 91.9°, and speed of 18.5 kt; and (b) P wake: 1637:57 UTC 27 Jul 2007, ship course of 342°, speed of 22.4 kt, wind direction of 120.7°, and speed of 12.9 kt. (bottom) Relative frequency (see the text) of S and P wakes as a function of relative wind direction (notice the sharp peaks about ±90°); angular bins are 20°. (c) S wakes and (d) P wakes.

sharp; the opposite port-side boundary is unclear (and/or much shorter than the former);
- ''P wakes'': only the port-side wake boundary is sharp; the starboard-side boundary is unclear (and/or much shorter than the former);
- ''B wakes'': both sides of the wake are sharp and have comparable lengths; and
- ''N wakes'': neither of the wake boundaries is sharp.

An example shown in Fig. 3 is an S wake.

b. Wake measurement

The dimensions of the wakes were measured from their photographic images. The location of the wake in the image may vary due to vibrations of the camera mount, vessel pitching, crabbing (nonzero angle between ship heading and the course), and other factors. The procedure outlined in this section is independent of these variations because the horizon line is used as a reference for distance measurements. However, this procedure requires that the horizon line and two ship wake boundaries can be seen clearly (e.g., Fig. 3).

Custom software has been developed that puts markers on the image and allows the operator to move these markers over the image, thus defining the position of the horizon and the edges of the visible wake. In our procedure (see Fig. 4), the horizon line (dark blue) is set first, and then 10 lines are automatically drawn parallel to the horizon line. Next, the operator places the markers at the outermost points of the intersection of each of these lines with the wake, thus defining a set of intervals (red lines). The distance from the center of an interval to the camera is denoted

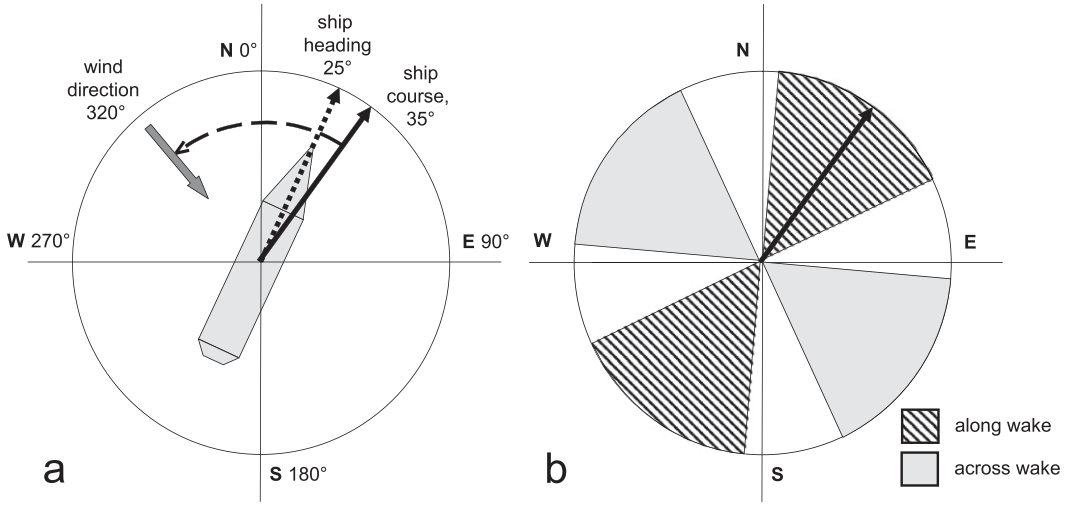

FIG. 6. An example illustrating the angular notations used in this study. Wind direction is specified according to meteorological conventions. (a) The angle corresponding to the ''wind direction relative to ship course'' is shown (curved arrow); the value of this angle is given by the difference of wind direction (320°) and ship course (35°); wrapped to the (−180°, 180°) interval, the value will be −75°. (b) For the same ship course of 35°, the hatched area is the range of wind directions called ''wind along the wake'' (from 5° to 65° and from 185° to 245°), the grayed area is the ''wind across the wake'' (from 95° to 155° and from 275° to 335°); see section 4b.

as L, and the interval length, which is the same as the full wake width at this distance, as W; these values can be calculated using the distance to the horizon line α_p and width β_p measured in the image (see Fig. 4). Thus, the shape of the wake is represented by a set of pairs (L, W) with 10 (or less) pairs per wake.

The formulas calculating L and W from α_p and β_p are given in the appendix. The derivation of these formulas

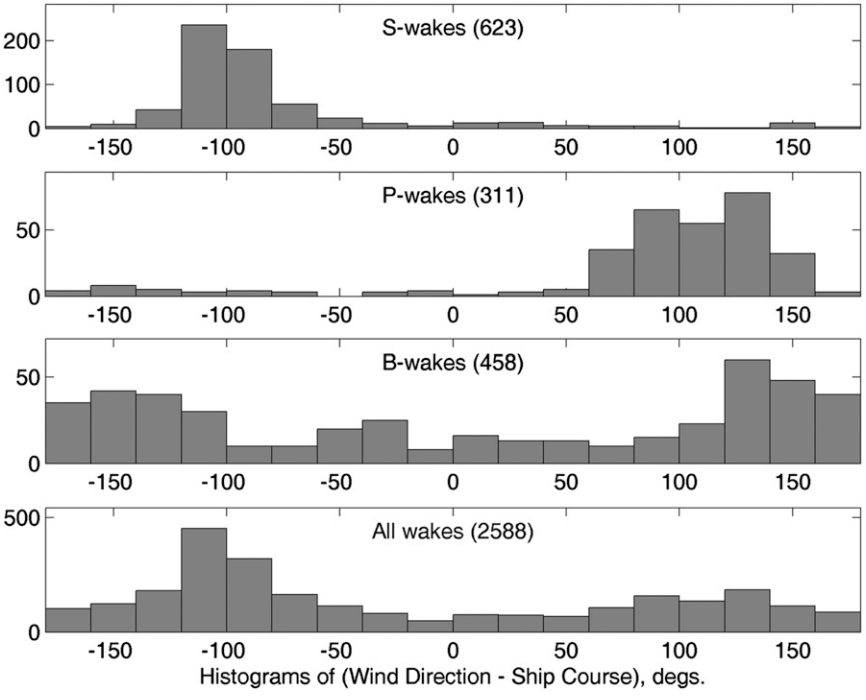

FIG. 7. Histograms for wind direction relative to the ship course for ship speed >7 kt. The numbers in parentheses show the total number of images for each histogram. The top two histograms demonstrate the asymmetry in the frequency of sharp wake boundaries with respect to wind direction. The ''All wakes'' histogram shows the asymmetry of relative wind direction for the dataset.

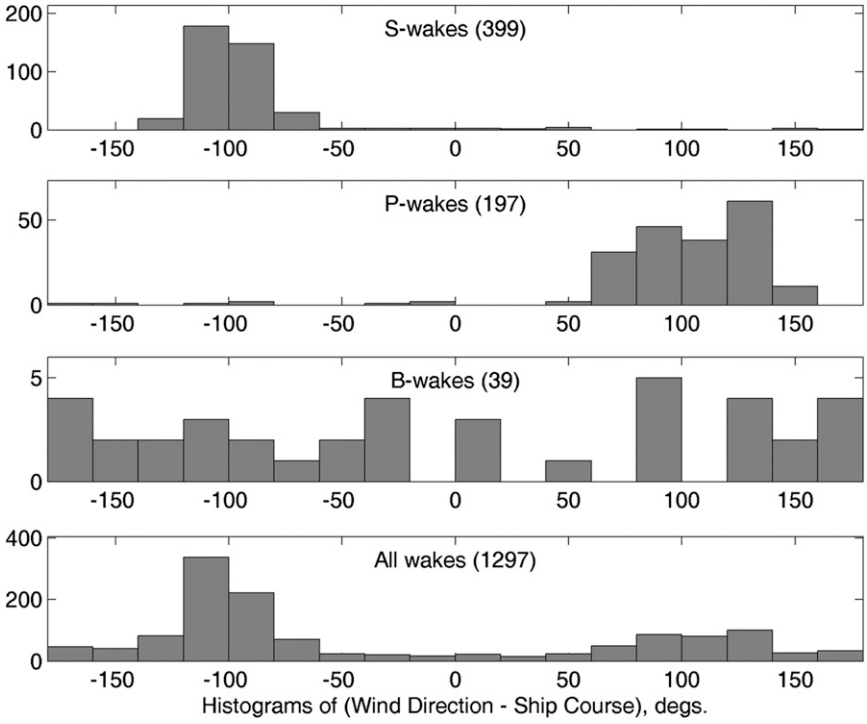

FIG. 8. As in Fig. 7, but with an additional condition of wind speed >15 kt. Note the disproportionately small number of B wakes.

is straightforward, although the expressions are bulky. A field validation of the wake measurement routines has been carried out using the photographs of navigation buoys near the Bermuda Islands during one of the *Explorer of the Seas* cruises. The validation was based on measuring distances to the same buoy in two consecutive images. The increment of distance obtained from two adjacent photographs was divided by the average ship velocity known from the ship's telemetry. The resulting time estimate was compared to the known interval between the image captures. The test has shown relatively good performance (within 2%) of the formulas used for calculation of the distance from camera.

4. Results and discussion

a. Wake asymmetry and wind direction

We have studied the correlation between wake asymmetry and relative wind direction. Figures 5a,b demonstrate examples of S and P wakes, respectively. The wake asymmetry is found to be strongly correlated to the wind direction relative to the ship course (the angles are explained in Fig. 6a). The relative frequency of S and P wakes in each angular bin is plotted in Figs. 5c,d. To obtain this data, the histogram values in the top two panels of Fig. 7 have been ''divided'' (normalized) by those in the bottom panel of Fig. 7. The plots in Figs. 5c,d show that if only one boundary of the wake is sharp, it is more often the leeward (downwind) boundary than the opposite (Soloviev et al. 2008). This asymmetry effect seems to be also sensitive to the wind speed: for the wind speeds above 15 kt, the above correlation persists, and the number of B wakes drops dramatically (see Fig. 8).

These observations suggest that wake asymmetry can be a result of wind–wake interaction. The wake asymmetry with respect to the wind direction may also be related to the interaction of the ship's superstructure with wind and the compensation of this interaction by the ship's Azipod propulsion system (Mattila et al. 2002). The wind–wake interaction hypothesis is more plausible because there are indications that specific features of the propulsion jets disappear in the far wake (Reed and Milgram 2002).

In the dataset under consideration, there are 648 S wakes, 311 P wakes, and 465 B wakes (out of a total 2588). The reason for dominance of S wakes over P wakes is not clear; one possible reason is, again, the asymmetry of the *Explorer of the Seas*' Azipod propulsion system. Another possible reason is the prevailing wind patterns and navigational routes. According to the diagram in Fig. 7 (lower panel), the ship more often experienced winds from the port side of the ship (1587 cases are conducive to S wakes versus the 1001 conducive to P wakes).

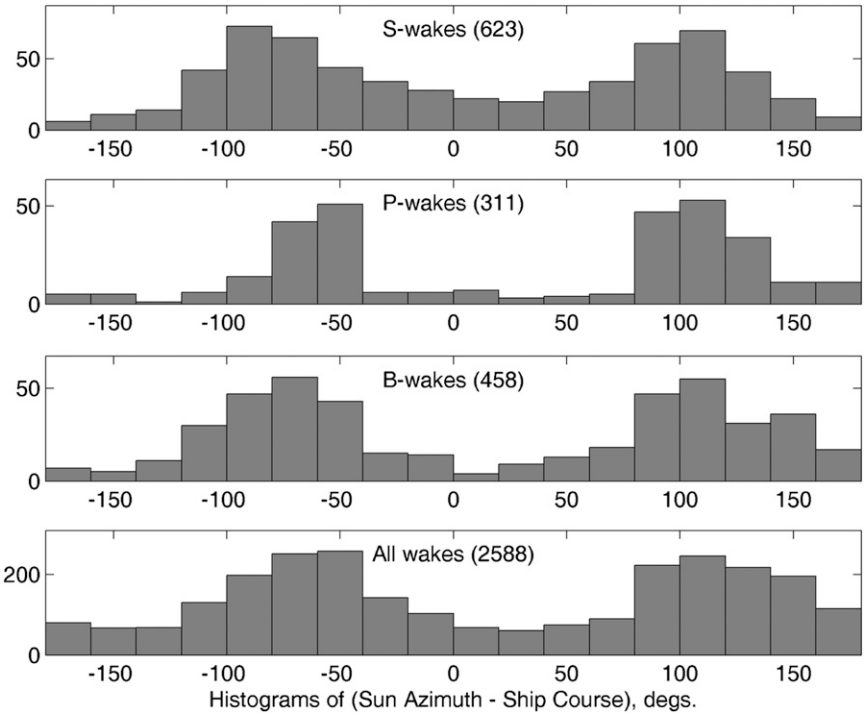

FIG. 9. Histograms for sun azimuth relative to the ship course for asymmetrical and symmetrical wakes, for ship speed >7 kt: The distribution patterns in the top two panels are similar, which excludes illumination effects as a possible cause of the asymmetry in Figs. 7 and 8. The angles near ±90° dominate in these histograms because the low latitudes and meridional directions prevail in the tracks of the *Explorer of the Seas* during the experiment.

Arguably, the optical visibility of a wake, and of a wake boundary in particular, may be either reduced or enhanced by illumination conditions, of which the relative position of the sun seems to be the most important factor. However, from the histograms in Fig. 9, no correlation between the wake asymmetry and sun position relative to ship course could be seen. An example where the effect of visibility is important is shown in Fig. 10. As explained in section 3b, our ability to apply the procedure illustrated by Fig. 4 depends on the visibility (i.e., visual contrast) of the wake

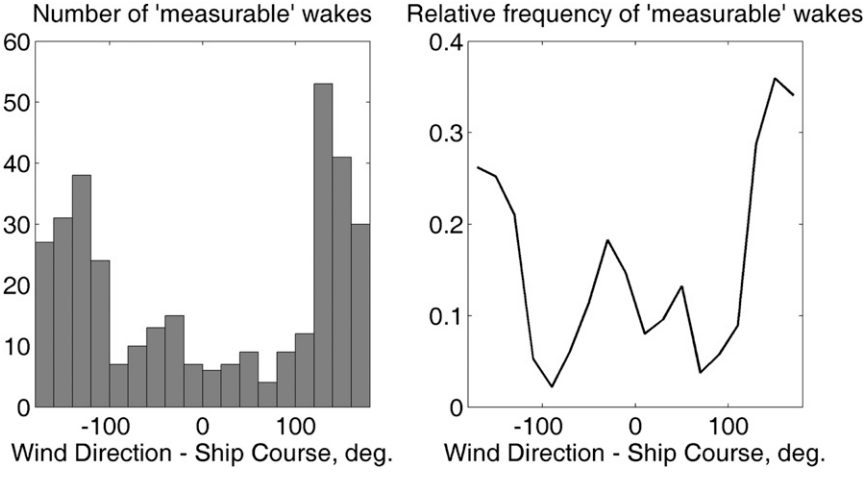

FIG. 10. (left) Histogram and (right) relative frequency of well-outlined (‘‘measurable’’) wakes vs relative wind direction, for ship speed >7 kt. The relative frequency data are defined as the values of the histogram divided (normalized) by the values of the ‘‘All wakes’’ panel in Fig. 7.

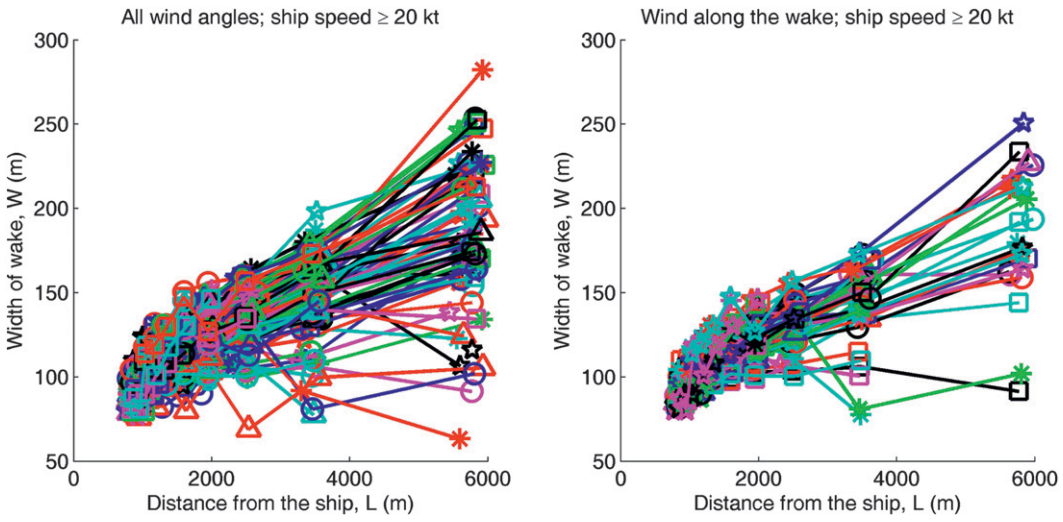

FIG. 11. Wake width vs distance plots for (left) all measured wakes and (right) relative wind direction within 30° of the ship track. Ship speed ranges from 20 to 24.4 kt.

boundaries. It turns out that for across-track winds (with a relative wind direction of around ±90°), it is possible to measure the wakes in less than 5% of images, whereas for following winds (±180°), this proportion exceeds 20%. The explanation of this phenomenon is beyond the scope of this article; it is only necessary to say here that the lack of a strong asymmetry in the relative frequency plot (Fig. 10, right) is another argument supporting the statement that the asymmetry in Figs. 5, 7, and 8 is not due to illumination factors.

b. Statistics of wake shape

Our dataset contains a total of 313 images for which it has been possible to perform the wake measurement as described in section 3b. Of these, only 11 images (3.5%) correspond to ship speed below 18 kt, and 51 more (16.3%) correspond to a ship speed interval from 18 to 20 kt. We see that the ''measurable'' wake images are concentrated in a narrow interval of ship speeds either at or just below the cruise speed of the *Explorer of the Seas*, which is 23 kt. For further analysis, we only select the images corresponding to ship speeds above 20 kt.

The wake width W as a function of distance to camera L is taken as a characteristic of the wake shape. For our analysis, we introduce two angular subsets of ''wind direction relative to the ship course'' (see Figs. 6a,b). The ''wind along the wake'' subset consists of two sectors, each of which is 60° wide and centered with the ship track. The ''wind across the wake'' subset consists of two similar sectors oriented perpendicularly to the ship track. The left panel of Fig. 11 plots $W = W(L)$ for all wind directions, while the right panel shows the same for the ''wind along the wake''. At distances exceeding 2 km from the ship, the width data exhibit significant scatter, which is probably related to the measurement techniques.

Figure 12 shows the average width (with a confidence interval of 95%) versus distance from the ship for all wind directions, as well as for the two angular subsets defined above. In both cases we see a slow monotonic increase of the average wake width as distance to the ship increases. The data show that in the ''wind along the wake'' case, the wake is slightly narrower than that in the ''wind across the wake'' case. This can be explained by the effect of the wind–wake interaction, which may result in not only the ship wake asymmetry (discussed in the previous section), but also the wake widening when the wind stress acts across the wake.

It is worthwhile pointing out that for the measurement of the ship wake width from a photo image, both wake

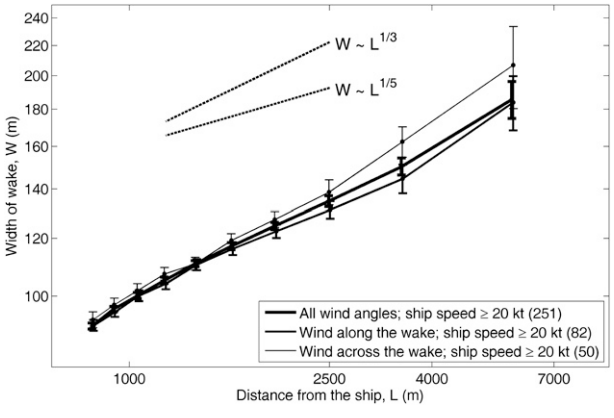

FIG. 12. Average wake width with 95% confidence intervals; the first two datasets are shown in Fig. 11. The number of images in each dataset is given in parentheses.

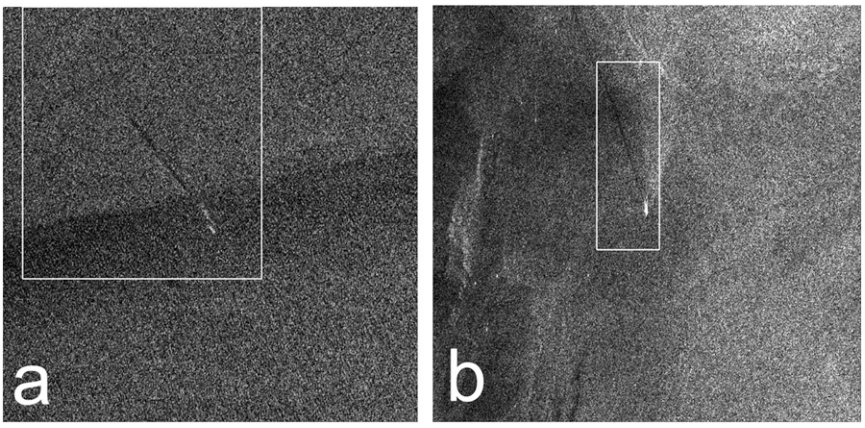

FIG. 13. The SAR images of the *Explorer of the Seas*. (a) RADARSAT S1 beam (12.5-m resolution), at 1051:34 UTC 21 May 2007; 37.6114°N, 70.3133°W; and speed of 21.6 kt, course of 133.4°, wind speed of 14.8 kt, and direction of 314.4°. (b) *RADARSAT* ScanSAR (25-m resolution), image from 1041:42 UTC 8 Sep 2007, ship at 41.0939°N, 69.2078°W, speed of 10.6 kt, course of 151.6°, wind speed of 20.2 kt, and direction of 238.9°.

boundaries should be visible. However, when wake asymmetry is strong, the contrast of the upwind boundary may be insufficient for a reliable detection and positioning of the upwind boundary in a photo image. This might be a contributing factor to the large scatter in the wake shape data.

For the empirical scaling of the dependence of wake width W on the distance L from the ship,

$$W \sim L^q, \tag{1}$$

the value of q characterizes the rate of spatial expansion of the wake. This rate has been the subject of multiple studies; however, the value of the exponent q in (1) varies from one case to another. For example, in the experiments involving measurements of surface tension in the wakes of surface ships (Peltzer et al. 1992), these values are between $1/6$ and $1/3$. The field measurements of the concentration of chemicals released in the ship wake (Katz et al. 2003) give values of q from 0.25 to 0.31, while numerical experiments in the same work report the values in the range of 0.18–0.2. In Weber et al. (2005), the observed $W(L)$ data are fitted with a second-degree polynomial, which results in values of q that are close to ½.

In Fig. 12, two extra segments of dashed lines show that in the present study, the results are better described by the value of $q = 1/3$. The scatter in the results of the wake expansion rate measurements may originate from several sources. First, wake shape may be affected by differences in meteorological conditions, ship operation parameters, and ship hull types. Second, the wake visible in photographic images (this study) does not necessarily coincide with that revealed by measurements of other parameters (Peltzer et al. 1992; Katz et al. 2003; Weber et al. 2005).

c. *Features of far ship wakes in optical and SAR imagery*

The ship wake asymmetry with respect to the wind–wake angle (see above) has also been observed in high-resolution synthetic aperture radar (SAR) satellite images (Lyden et al. 1988; Wahl et al. 1992; Soloviev et al. 2010). The asymmetry in SAR images often has the form of "a bright edge on the upwind side" of the dark wake and is explained by the hydrodynamic modulation of short surface waves at the wake edge (Lyden et al. 1988; Fujimura et al. 2010).

It is interesting to compare the shape of the wakes in photographs taken from the ship and in satellite SAR imagery. Figure 13 (with fragments shown in Figs. 14 and 15) presents two SAR images of the wake of the *Explorer of the Seas* obtained from the *RADARSAT-1* satellite. The big bright speckle is the *Explorer of the Seas*. The centerline wake appears as a dark scar resulting from the suppression of roughness by the wake currents and surface films (Reed and Milgram 2002).

The SAR image shown in Figs. 13a and 14 is a "wind along the wake" case, while the SAR image shown in Figs. 13b and 15 is a "wind across the wake" case. Note that the spatial resolution of the *RADARSAT-1* image in "wind across the wake" case (Figs. 13b and 15) is 25 m, which is not sufficient to resolve the asymmetry resulting from wind–wake interaction. The pairs of white dots in Figs. 14 and 15 are superimposed on the image at the positions corresponding to the averaged experimental values of (W, L) pairs obtained from the *Explorer of the Seas* photographic measurements (Fig. 12). While these two cases represent different ship speeds, the shape of both wakes in radar images is consistent with the averaged shape measured from the photographic images.

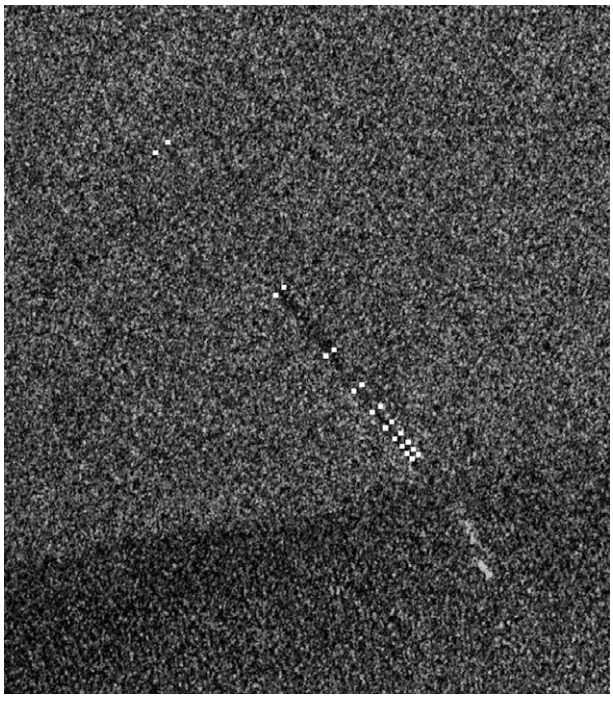

FIG. 14. Fragment from Fig. 13a. Average wake width calculated from photographic measurements (white dots; Fig. 12, wind along the wake curve).

Figure 16a demonstrates 10 cross sections through the centerline wake shown in Fig. 14, with the dashed lines showing the average wake width obtained from the photographic images. An average of the profiles in Fig. 16a is plotted in Fig. 16b. These plots suggest a good correlation between satellite- and ship-based measurements.

5. Conclusions

We have presented an experimental methodology aimed at studying ship wakes from photographic imagery. Through the installation of a photographic camera on a large cruise ship, we have collected and analyzed a dataset consisting of more than 2500 images. A wake shape measurement procedure has been developed, as well as an analysis of the wake asymmetry based on the visibility of wake boundaries. These approaches proved to be effective in establishing the links between the geometric properties of the wake and the wind speed and direction. It has been demonstrated that the longer and better seen wake boundary is more likely to be on the downwind side. There is good agreement between the averaged shape of the wakes measured from the photographic images and the few available satellite-based radar images of the wake of the same ship.

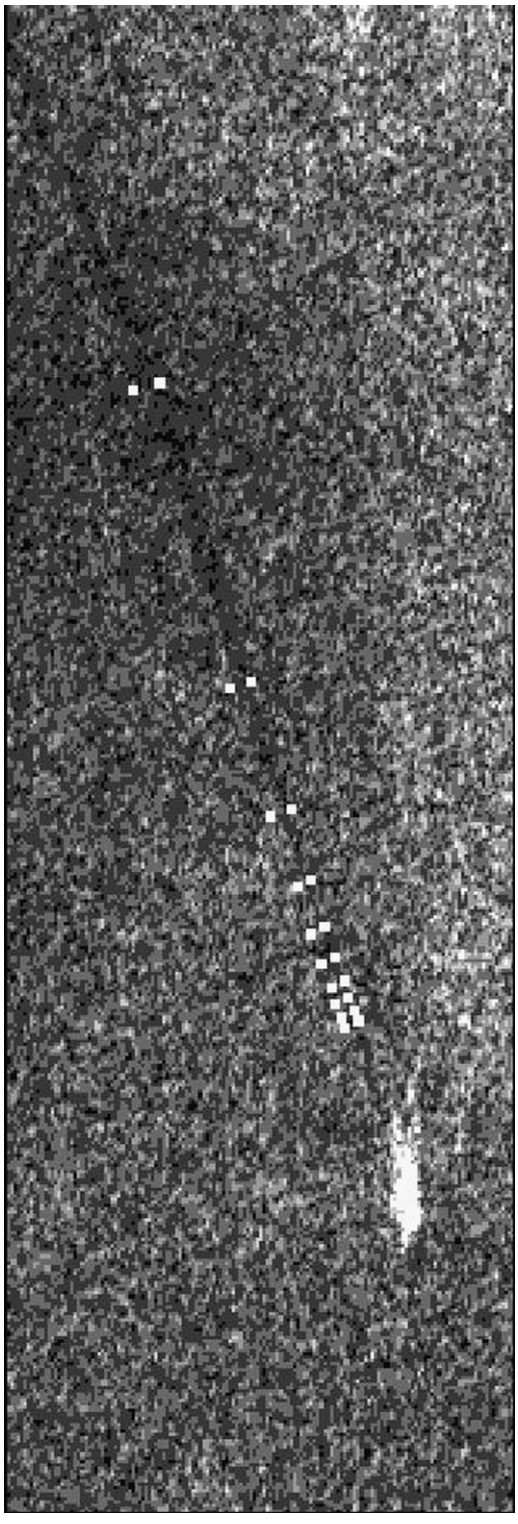

FIG. 15. Fragment from Fig. 13b. Average wake width calculated from photographic measurements (white dots; Fig. 12, wind across the wake curve).

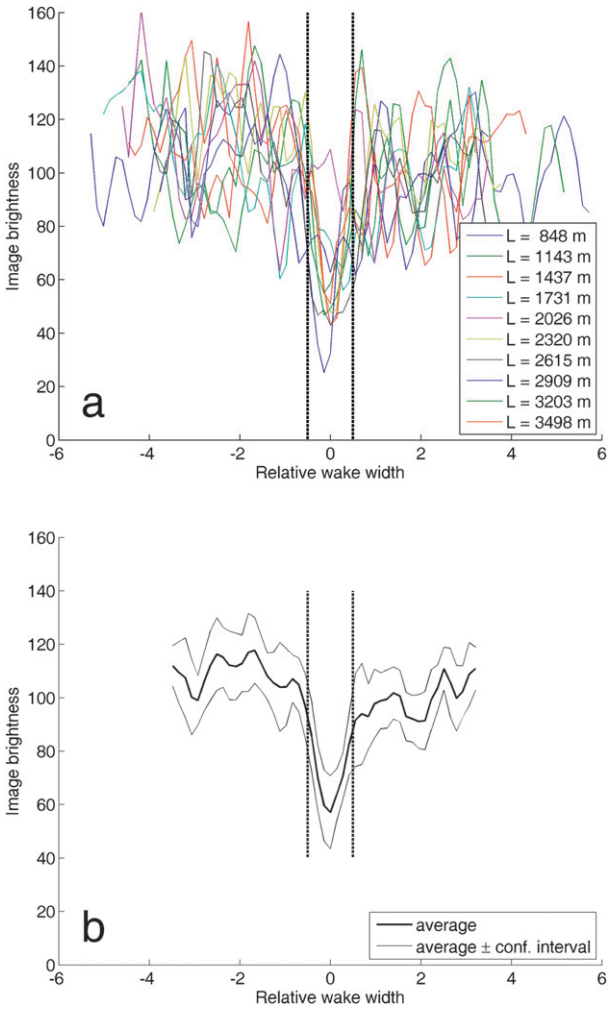

FIG. 16. (a) Ten cross-wake plots of image brightness (arbitrary units) through the visible centerline wake in Fig. 14 after 3 × 3 median filtering and additional 5 × 1 averaging along the wake. Each color corresponds to a certain distance from the ship, while the across-wake distance is normalized by the average wake width (Fig. 12, "wind along the wake" curve) at this distance. The dashed vertical lines plotted at abscissa values ±0.5 represent the normalized wake width in photographic measurements. (b) Average and 95% confidence interval of cross-wake plots in (a).

Acknowledgments. Discussions with Mike Portnoff, Ursula Goldstein (LLNL), and Karen Fisher (LANL) were very helpful for outlining the recent status of the ship wake problem. Katherine Moore and Kathryn Young (both NSU OC students at the time of the experiment) have provided significant technical help with installation of the camera and data processing, including the wake measurements. We acknowledge UM RSMAS and *Royal Caribbean International* for accommodating our experiment on the *Explorer of the Seas*. We thank Dr. Peter Ortner, Elizabeth Williams, Chip Maxwell, Don Cucchiara (all at UM RSMAS), and Terry Thompson (NSU OC) for help in conducting the experiment on the *Explorer of the Seas*, and Paul Mallas (UM RSMAS) for help in finding satellite-based radar images of the wake of the *Explorer of the Seas*. We are grateful to Dr. Silvia Matt (UM RSMAS) for useful discussions of the project results, and to Kate Vella and Christopher Maingot (both at NSU OC) for reading and improving the style of the manuscript. The comments by anonymous reviewers have been useful for improving the presentation of this paper. This work has been supported by the NSU Oceanographic Center from the project "Hydrodynamics and Remote Sensing of Far Wakes of Ships" and by the University of Miami RSMAS project "Center for Southeastern Tropical Advanced Remote Sensing" funded by the Office of Naval Research under Grant N00014-06-1-0931.

APPENDIX

Measurements of Wake Dimensions

The calculation of the distance from the camera L and the full wake width W starts from the calculation of the distance to the horizon line α_p and length of the interval β_p (see Fig. 4). The angular value of one pixel is calculated from the field-of-view angle of the lens (9° diagonal) and the image size in pixels (3872 × 2592 at maximum resolution). Thus, for each interval, the following two angles are calculated: angular distance to the horizon line α and angular width β.

To obtain the values of L and W from α and β, the following values are also needed: the height of camera position H, earth radius R, and line-of-sight curvature ρ resulting from atmospheric refraction. There is a multitude of formulas for calculating L from α: at least five formulas are listed or referenced in Kinzey and Gerrodette (2003). For the ease of validation, however, we present a derivation of an alternative set of formulas. All these formulas may differ slightly by their account of refraction and the definition of L, which may be the exact slant distance or its projection on the local horizon (as in our paper), etc. For this experiment, all of the measured distances were much larger than the camera height and much smaller than the earth's radius, so the difference between the slant distance and its projection can be ignored. The account of refraction, however, proved to be significant, especially for the measurements closest to the horizon.

In absence of atmospheric refraction, the lines of sight are straight (see Fig. A1). For a given α, the equation of the line of sight in the coordinates chosen is

$$y = H - kx. \tag{A1}$$

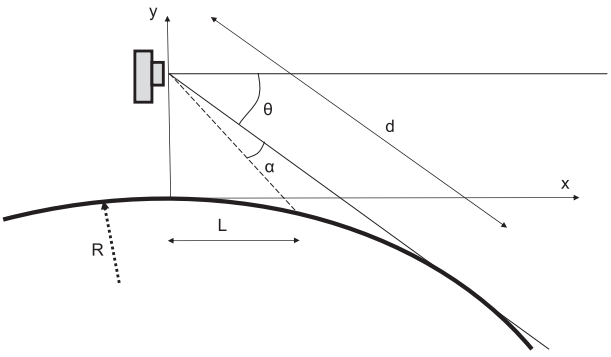

FIG. A1. Line-of-sight geometry in absence of refraction.

Here, $k = \tan(\alpha_T) = \tan(\alpha + \theta)$; α_T is the line-of-sight dip angle measured from the local horizon, θ is the horizon dip angle defined as

$$\tan\theta = d/R, \tag{A2}$$

with the tangent length d given by

$$d^2 = H(2R + H). \tag{A3}$$

The earth's surface is a sphere described by the equation

$$x^2 + (y + R)^2 = R^2. \tag{A4}$$

Exclusion of y from (A1) and (A4) leads to a quadratic equation

$$ax^2 + bx + c = 0, \tag{A5}$$

where

$$a = 1 + k^2; \quad b = -2k(R + H); \quad c = H(H + 2R). \tag{A6}$$

The lowest of two roots of this quadratic equation gives L.

In presence of atmospheric refraction, the lines of sight are circles with some radius ρ (see Fig. A2), their equations given in adapted coordinate frame [cf. (A4)]

$$x_T^2 + (y_T + \rho)^2 = \rho^2. \tag{A7}$$

The initial and adapted coordinates are related by

$$x = x_T \cos\alpha_T + y_T \sin\alpha_T,$$
$$y = H - x_T \sin\alpha_T + y_T \cos\alpha_T.$$

Excluding y from (A4) and (A7) we get the equation for the abscissa of the intersections of the line of sight with

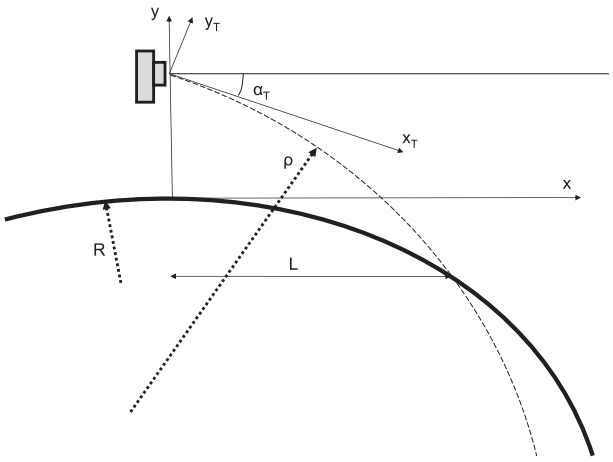

FIG. A2. Line-of-sight geometry with refraction.

the earth's surface. The resulting equation is similar to (A5), with

$$a = 1 + B^2; \quad b = 2B(A + R); \quad c = A(A + 2R), \tag{A8}$$

where

$$A = (H^2 - 2\rho H \cos\alpha_T)/2(R + H - \rho\cos\alpha_T);$$
$$B = \rho \sin\alpha_T/(R + H - \rho\cos\alpha_T). \tag{A9}$$

The value of L is again the lowest of two roots of this quadratic equation, with coefficients depending on α_T. The calculation of α_T involves θ, which can be defined now as the dip of the line-of-sight tangent to the earth's surface (see Fig. A3).

One of the ways to calculate θ in the presence of refraction makes use of the fact that the line going through the centers of two tangent circles also goes through the tangent point. Thus, the center of such a line-of-sight circle is located at the distance ρ from the camera and at the distance $(\rho - R)$ from the earth's center (Fig. A3). This gives us the following two equations for the center's coordinates:

$$x_C^2 + (y_C - H)^2 = \rho^2,$$
$$x_C^2 + (y_C + R)^2 = (\rho - R)^2.$$

Solving these, the following expression for θ is obtained instead of (A2):

$$\tan^2\theta = x_C^2/(y_C - H)^2 = H \cdot C \cdot D/E^2, \tag{A10}$$

where

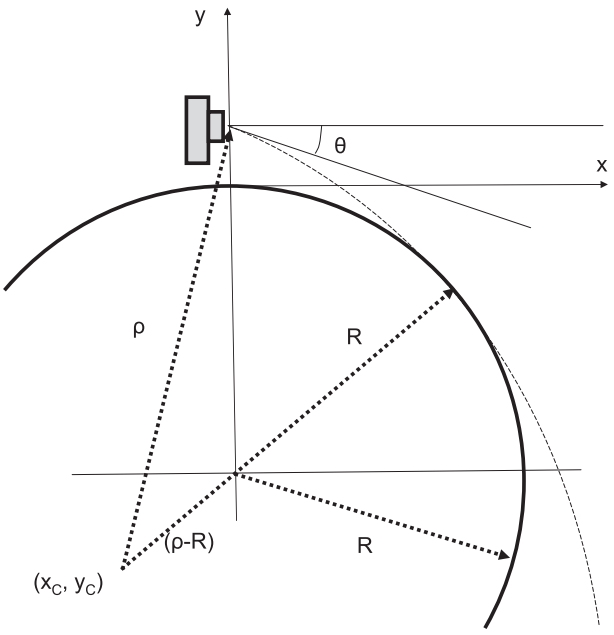

FIG. A3. Calculations of tangent line of sight with refraction.

$$C = 1 - (R/\rho) - (H/2\rho);$$
$$D = 2R + H + (HR/\rho) + (H^2/2\rho);$$
$$E = R + (HR/\rho) + (H^2/2\rho). \quad \text{(A11)}$$

For calculation of the line-of-sight curvature ρ as a function of a vertical temperature gradient γ (sometimes also called the ''lapse rate''), the following simple formula was used:

$$\frac{1}{\rho} = 7.5 + 2.2 \cdot \gamma, \quad \text{(A12)}$$

where $1/\rho$ and γ are expressed in arc seconds per kilometer and in kelvins per hundred meters, respectively (see, e.g., Lehn 1979). The typical values of γ are negative; either the ''dry adiabatic lapse rate'' of $\gamma = -1$ or the average experimental $\gamma = -0.65$ could be taken (Wallace and Hobbs 1977). For Figs. 11 and 12 in this paper, the value $\gamma = -0.65$ was used. As $\rho \to \infty$, Eqs. (A10) and (A11) reduce to (A2), and Eqs. (A8) and (A9) reduce to (A6).

After the distance L is calculated, the width W is expressed as

$$W = 2L \tan\beta/2.$$

Repeating the calculations of L and W for each measurement line on the image results in a set of pairs that represent the function $W = W(L)$ displayed in Fig. 11.

REFERENCES

Benilov, A., G. Bang, A. Safray, and I. Tkachenko, 2001: Ship wake detectability in the ocean turbulent environment. *Proc. 23rd Symp. on Naval Hydrodynamics,* Val de Reuil, France, Office of Naval Research and Cosponsors, 1–15.

Brown, E. D., S. Buchsbaum, R. E. Hall, J. P. Penhune, K. F. Schmitt, K. M. Watson, and D. C. Wyatt, 1989: Observations of a nonlinear solitary wavepacket in the Kelvin wave of a ship. *J. Fluid Mech.,* **204,** 263–293.

Crisp, D. J., 2004: The state-of-the-art in ship detection in synthetic aperture radar imagery. DSTO Information Sciences Laboratory, Australian Department of Defense Rep. DSTO-RR-0272, 116 pp. [Available online at http://dspace.dsto.defence.gov.au/dspace/bitstream/1947/3354/1/DSTO-RR-0272%20PR.pdf.]

Eldhuset, K., 1996: An automatic ship and ship wake detection system for spaceborne SAR images in coastal regions. *IEEE Trans. Geosci. Remote Sens.,* **34,** 1010–1019.

Fu, L. L., and B. Holt, 1982: Seasat views oceans and sea ice with synthetic-aperture radar. NASA Jet Propulsion Laboratory Publ. 81-120, 200 pp.

Fujimura, A., A. Soloviev, and V. Kudryavtsev, 2010: Numerical simulation of the wind stress effect on SAR imagery of far wakes of ships. *IEEE Geosci. Remote Sens. Lett.,* **7,** 646–649.

Garrett, W. D., and P. M. Smith, 1984: Physical and chemical factors affecting the thermal IR imagery of ship wakes. Naval Research Laboratory Memo. 5376, 29 pp.

Greidanus, H., and N. Kourti, 2006: Findings of the DECLIMS project—Detection and classification of marine traffic from space. *Proc. SEASAR 2006: Advances in SAR Oceanography from ENVISAT and ERS Missions,* Rome, Italy, European Space Agency. [Available online at http://earth.esa.int/seasar06/proceedings/papers/87_greidanus.pdf.]

Hyman, M., 2000: Computation of ship wake flows with free-surface/turbulence interaction. *22nd Symp. on Naval Hydrodynamics,* Vol. 22, Washington, D.C., ODR, 835–847.

Katz, C. N., D. B. Chadwick, J. Rohr, M. Hyman, and D. Ondercin, 2003: Field measurements and modeling of dilution in the wake of a US navy frigate. *Mar. Pollut. Bull.,* **46,** 991–1005.

Kinzey, D., and T. Gerrodette, 2003: Distance measurements using binoculars from ships at sea: Accuracy, precision and effects of refraction. *J. Cetacean Res. Manage.,* **5,** 159–171.

Lehn, W. H., 1979: The Novaya Zemlya effect: An arctic mirage. *J. Opt. Soc. Amer.,* **69,** 776–781.

Lyden, J. D., R. R. Hammond, D. R. Lyzenga, and R. A. Schuchman, 1988: Synthetic aperture radar imaging of surface ship wakes. *J. Geophys. Res.,* **93,** 12 293–12 303.

Mattila, M., J. Ylitalo, and J. Soles, 2002: Semisubmersible rig—The reliable solution with minimal thrust losses. *Dynamic Positioning Conf.,* Houston, TX, Marine Technology Society. [Available online at http://www.dynamic-positioning.com/dp2002/design_azipod_propulsion.pdf.]

Munk, W. H., P. Scully-Power, and F. Zachariasen, 1987: The Bakerian lecture, 1986: Ships from space. *Proc. Roy. Soc. London,* **412A,** 231–254.

Peltzer, R. D., O. M. Griffin, W. R. Barger, and J. A. C. Kaiser, 1992: High-resolution measurements of surface-active film redistribution in ship wakes. *J. Geophys. Res.,* **97,** 5231–5252.

Reed, A. M., and J. H. Milgram, 2002: Ship wakes and their radar images. *Annu. Rev. Fluid Mech.,* **34,** 469–502.

Soloviev, A., M. Gilman, K. Moore, K. Young, and H. Graber, 2008: Hydrodynamics and remote sensing of far wakes of ships. *SEASAR 2008—Second Int. Workshop on Advances in SAR Oceanography,* Frascati, Italy, European Space Agency. [Available online at http://earth.esa.int/workshops/seasar2008/participants/187/pres_187_soloviev.pdf.]

——, ——, K. Young, S. Brusch, and S. Lehner, 2010: Sonar measurements in ship wakes simultaneous with TerraSAR-X overpasses. *IEEE Trans. Geosci. Remote Sens.,* **48,** 841–851, doi:10.1109/TGRS.2009.2032053.

Soomere, T., 2007: Nonlinear components of ship wake waves. *Appl. Mech. Rev.,* **60,** 120–138.

Vachon, P. W., 2006: Ship detection in synthetic aperture radar aperture imagery. *Proc. OceanSAR 2006—Third Workshop on Coastal and Marine Applications of SAR,* St. John's, NL, Canada, Earth Observation Marine Surveillance Coordination Committee. [Available online at http://www.oceansar2006.com/papers/82_Vachon_Oceansar2006.pdf.]

Wahl, T., K. Eldhuset, and A. Skøelv, 1992: Ship traffic monitoring using the ERS-1 SAR. *Proc. First ERS-1 Symp.,* Cannes, France, ESA, SP-359.

Wallace, J. M., and P. V. Hobbs, 1977: *Atmospheric Science—An Introductory Survey*. Academic Press, 467 pp.

Weber, T. C., A. P. Lyons, and D. L. Bradley, 2005: An estimate of the gas transfer rate from oceanic bubbles derived from multibeam sonar observations of a ship wake. *J. Geophys. Res.,* **110,** C04005, doi:10.1029/2004JC002666.

Zheng, Q., X.-H. Yan, W. T. Liu, V. Klemas, and D. Sun, 2001: Space shuttle observations of open ocean oil slicks. *Remote Sens. Environ.,* **76,** 49–56.

Zilman, G., A. Zapolski, and M. Marom, 2004: The speed and beam of a ship from its SAR wake images. *IEEE Trans. Geosci. Remote Sens.,* **42,** 2335–2342.